



**HAL**  
open science

## Homogenization of periodic 1-3 piezocomposite using wave propagation: Toward an experimental method

Antoine Balé, Rémi Rouffaud, Franck Levassort, Renald Brenner,  
Anne-Christine Hladky

► **To cite this version:**

Antoine Balé, Rémi Rouffaud, Franck Levassort, Renald Brenner, Anne-Christine Hladky. Homogenization of periodic 1-3 piezocomposite using wave propagation: Toward an experimental method. *Journal of the Acoustical Society of America*, 2021, 149 (5), pp.3122-3132. 10.1121/10.0004824 . hal-03227151

**HAL Id: hal-03227151**

**<https://hal.science/hal-03227151>**

Submitted on 17 May 2021

**HAL** is a multi-disciplinary open access archive for the deposit and dissemination of scientific research documents, whether they are published or not. The documents may come from teaching and research institutions in France or abroad, or from public or private research centers.

L'archive ouverte pluridisciplinaire **HAL**, est destinée au dépôt et à la diffusion de documents scientifiques de niveau recherche, publiés ou non, émanant des établissements d'enseignement et de recherche français ou étrangers, des laboratoires publics ou privés.

# Homogenization of periodic 1-3 piezocomposite using wave propagation: toward an experimental method

Antoine Balé,<sup>1, a</sup> Rémi Rouffaud,<sup>1, b</sup> Franck Levassort,<sup>1</sup> Renald Brenner,<sup>2</sup> and

Anne-Christine Hladky-Hennion<sup>3</sup>

<sup>1</sup>*GREMAN UMR7347, University of Tours, CNRS, INSA-CVL, 37100 Tours, France*

<sup>2</sup>*Sorbonne Université, CNRS, UMR 7190, Institut Jean Le Rond d'Alembert, F-75005 Paris, France*

<sup>3</sup>*CNRS, Centrale Lille, ISEN, Univ-Lille, Univ-Valenciennes, UMR8520-IEMN, 59000 Lille, France*

(Dated: 17 May 2021)

1 1-3 piezocomposites are first choice materials for integration in ultrasonic transduc-  
2 ers due to their high electromechanical performance, particularly in their thickness  
3 mode. The determination of a complete set of effective electroelastic parameters  
4 through a homogenization scheme is of primary importance for their consideration as  
5 homogeneous. This allows for the simplification of transducer design using numeri-  
6 cal methods. The method proposed is based on acoustic wave propagation through  
7 infinite piezocomposite that are considered homogeneous material. Christoffel tensor  
8 components for the 2mm symmetry were expressed to deduce slowness curves in sev-  
9 eral planes. Simultaneously, slowness curves of a numerical phantom were obtained  
10 using a Finite Element Method (FEM). Dispersive curves were initially calculated in  
11 the corresponding heterogeneous structure. Subsequent identification of the effective  
12 parameters was based on a fitting process between the two sets of slowness curves.  
13 Then homogenized coefficients were compared with reference results from a numerical  
14 method based on fast-Fourier transform (FFT) for heterogeneous periodic piezoelec-  
15 tric materials in the quasi-static regime. A relative error of less than 2% for a very  
16 large majority of effective coefficients was obtained. As the aim of the manuscript  
17 is to implement an experimental procedure based on the proposed homogenization  
18 scheme in order to determine the effective parameters of the material in operating  
19 conditions, it is shown that simplifications to the procedure can be performed and  
20 that a careful selection of only seven slowness directions is sufficient to obtain the  
21 complete database for a piezocomposite containing square shaped fibers. Finally,  
22 further considerations to adapt the present work to a 1-3 piezocomposite with fixed

thickness are also presented.

---

<sup>a</sup>Also at CNRS, Centrale Lille, ISEN, Univ-Lille, Univ-Valenciennes, UMR8520-IEMN, 59000 Lille, France

<sup>b</sup>[remi.rouffaud@univ-tours.fr](mailto:remi.rouffaud@univ-tours.fr)

## 24 I. INTRODUCTION

25 Piezoelectric composite materials are used in various applications such as sensors, ac-  
26 tuators and transducers. Among the many patterns of spatial distribution between the  
27 piezoelectric and inert phases, 1-3 connectivity, i.e., aligned piezoelectric rods embedded  
28 in a polymer matrix<sup>1</sup> for the corresponding piezocomposite (13PC), can deliver very high  
29 performance in the thickness mode<sup>2</sup>, leading to their application in ultrasonic transducers<sup>3</sup>.  
30 In order to design transducers integrating 13PCs, numerical methods such as Finite Dif-  
31 ference Method (FDM) or Finite Element Method (FEM) are commonly used. However,  
32 owing to the complexity of the studied system (number of phases, phase arrangement, mi-  
33 crostructure), tedious meshing is required when performing detailed modeling of 13PC.  
34 Moreover, depending on the target application the high precision levels achieved by such  
35 calculations are not always necessary. Users of numerical methods preferentially model these  
36 transducers with a 13PC simulated as a single-phase homogeneous material with effective  
37 properties. This theoretical step corresponding to a homogenization procedure is performed  
38 in the framework of the long-wavelength approximation and a subject that was extensively  
39 studied during the 1980s and 90s when piezocomposites, in particular, 13PC first became  
40 available. Typically, models were initially developed for purely elastic materials and sub-  
41 sequently extended to take into account the different coupling phenomena, in particular  
42 piezoelectricity.

43 The simplest approaches are those of Voigt<sup>4</sup> and Reuss<sup>5</sup> with uniform trial fields. These  
44 have been extended to piezoelectricity to obtain rigorous upper and lower bounds on the

45 effective free-energy<sup>6</sup>. In 1985, Banno derived an analytical expression for the calcula-  
46 tion of several effective material parameters for 13PC<sup>7</sup>, based on the model developed by  
47 Newnham<sup>1</sup>. Smith *et al.*<sup>2</sup> in addition, considered thickness mode effective parameters of  
48 13PC with analytical expressions. Other workers managed to determine additional effective  
49 parameters for all components of the three elastic, dielectric and piezoelectric tensors (elec-  
50 troelastic moduli) for the different piezocomposites<sup>8-11</sup>. However, the accuracy delivered  
51 for all parameters related to the thickness mode in these later approaches were not always  
52 congruent and very often remained proprietary, in particular parameters for 13PC.

53 At the end of the 1950's, Eshelby had considered the problem of an ellipsoidal inclusion  
54 embedded in an infinite matrix and had obtained the analytical expression of the stress and  
55 strain fields which turned out to be unchanged within the inclusion<sup>12</sup>. This fundamental  
56 result today forms the basis of several mean-field micromechanical models used to estimate  
57 the overall elastic moduli tensor. In 1980, Deeg<sup>13</sup> extended this solution to the calculation  
58 of coupled fields, in particular, piezoelectric materials. Dunn and Taya<sup>14</sup> proposed a method  
59 of obtaining effective parameters of a piezocomposite, as did various other workers<sup>15-17</sup>. In  
60 these configurations, 13PCs are a particular case of these models where one of the axes of  
61 ellipsoidal inhomogeneities tends toward infinity. FEM or more generally numerical methods  
62 are also used for 13PC homogenization. The main advantage of numerical methods is that  
63 there is no restriction on geometry, size, material parameters and number of phases in the  
64 structure<sup>18</sup>. With these methods, different boundary conditions (displacement and electrical  
65 potential) are applied to the Representative Volume Element (RVE) in order to determine  
66 mechanical and electrical fields inside the material. Details of such methods are given in

67 several reports<sup>19-26</sup>. Recently, the various homogenization methods presented above have  
68 also been adapted and applied to study novel 13PC in order to demonstrate their enhanced  
69 properties<sup>27,28</sup>

70 For all these models, the required input data are properties of the constituent phases  
71 and according to one of the methods briefly described above, this can vary from only a few  
72 parameters to the full set of electroelastic moduli for the piezoelectric phase. The effective  
73 parameters obtained by these homogenization procedures are therefor directly dependent  
74 upon these initial data. However, various 13PC fabrication processes (such as the "Dice  
75 and Fill" method<sup>29</sup>) introduce possible variations of properties for each phase and as a  
76 consequence variation on the final effective properties. Two examples can be highlighted:  
77 the machining process of the piezoelectric phase (starting typically from a bulk ceramic)  
78 to design the rods can degrade the piezoelectric properties while addition of the polymer  
79 around the rods introduces porosity (air bubbles) which modifies its mechanical properties.  
80 Beyond the development of accurate models, measurement of the piezocomposite parameters  
81 in *operating conditions* is essential. Characterization based on 13PC electrical impedance  
82 measurements was performed by us<sup>30</sup> and the objective of this present work is to develop a  
83 homogenization procedure based on acoustic wave propagation. This theoretical procedure  
84 was implemented with the understanding that it could then be applied by adapting it to an  
85 experimental set-up and thereby effects a correct estimation of homogenized parameters in  
86 *operating conditions*.

87 This approach used mechanical wave propagation through the 13PC and allowed extrac-  
88 tion of the effective parameters in a similar way to reported works for different configurations<sup>31-35</sup>.

89 This method as extended to piezoelectric materials, was inspired by Langlet *et al.*<sup>36</sup> who  
90 determined the effective tensor of porous elastic materials.

91 With the assumption of an infinite piezoelectric material, the behavior of wave propaga-  
92 tion is first presented for the two media of interest in section II. Then, in section III, slowness  
93 curves from homogeneous media are fitted on heterogeneous media with the analytical de-  
94 termination of some elastic parameters before optimization algorithms were used to deliver  
95 all the components of the effective electroelastic moduli. From this fit, a homogeneous  
96 equivalent medium is determined. In section IV, these results are compared with effective  
97 electroelastic coefficients obtained with a Fourier transform-based numerical scheme for pe-  
98 riodic piezoelectric materials in the quasi-static regime<sup>37-40</sup>. The same initial database for  
99 our numerical phantom was used. This comparison was essential and allowed us to validate  
100 our new procedure. The influences of two rod shapes and piezoelectric phase volume frac-  
101 tions on several effective parameters are discussed. Finally, with reference to experimental  
102 procedure, two essential points are addressed. First, minimization of the number of slow-  
103 ness values is examined while simultaneously maintaining accuracy on the deduced effective  
104 parameters. Finally, considerations aimed at adapting the present work to a piezoelectric  
105 medium with a given thickness and lateral dimensions, is put forward.

## 106 II. WAVE PROPAGATION IN AN INFINITE PIEZOELECTRIC MATERIAL

107 For a piezoelectric material, constitutive equations interacts the mechanical parameters  
108 (strain  $S$  and stress  $T$  tensors) with the electrical parameters (electric field  $E$  and electric  
109 displacement  $D$ ). In the framework of linear behavior, combining Maxwell equations and



110 Hooke's law, the interaction is written as follow<sup>41</sup>:

$$T_{ij} = c_{ijkl}^E S_{kl} - e_{ikl} E_i \quad (1)$$

$$D_i = \epsilon_{ij}^S E_j + e_{ikl} S_{kl}$$

111 where  $c^E$ ,  $e$  and  $\epsilon^S$  are, respectively, the elastic tensor at constant electric field, the piezo-  
112 electric tensor and the dielectric tensor at constant strain and subscripts  $i, j, k, l \in [1, 2, 3]$ ,  
113 the 3 space dimensions. Spatial directions 1, 2 and 3 are used indifferently throughout  
114 the text with directions X, Y and Z. In the long wavelength approximation, an anisotropic  
115 heterogeneous medium can be considered as an anisotropic homogeneous medium if size  
116 inhomogeneities are smaller than the selected wavelength<sup>42</sup>. With this assumption, the use  
117 of classical plane waves for the study of homogeneous medium in section II B is possible.

## 118 **A. Heterogeneous structure**

119 To study the wave propagation in a 13PC, FEM is used.

### 120 **1. FE model: 4mm- and mm2-structures**

121 In this work, two 13PC designs are investigated. The two were chosen because, from  
122 a practical point of view, both can be manufactured by the well-known "Dice and Fill"  
123 method<sup>29</sup>. In fig.1, top views of the two periodic configurations are shown with grey  
124 piezoelectric square-shaped rods (fig.1.(a))<sup>29</sup> or right-triangle (fig.1.(b))<sup>45</sup> shaped rods sur-  
125 rounded by polymer. To determine the effective symmetry of each structure, the rod-shaped  
126 piezoelectric material and the relative positioning of rods to each other, are taken into ac-

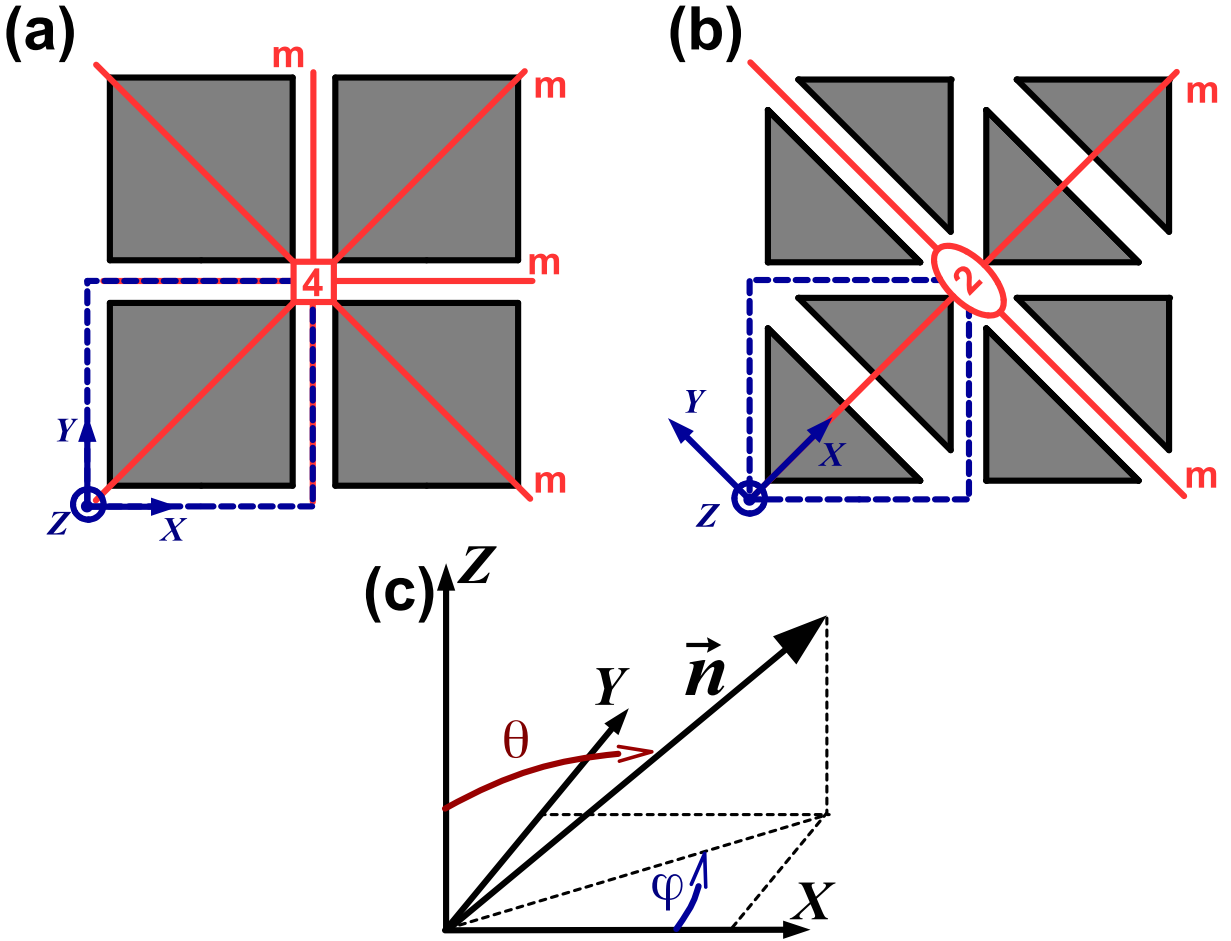


FIG. 1. Top view of elementary 13PC patterns for a) 4mm and b) mm2 symmetries. Surrounded in blue line, are RVEs meshed with FEM with the local orthonormal basis ( $XYZ$ ). c) Unit propagation vector  $\vec{n}$  is defined by angles  $\theta$  and  $\varphi$  in the local basis. Grey areas represent the piezoelectric rods surrounded by a polymer.

127 count. In the case of Fig1.(a), 4-fold axis of symmetry exists (red square at center of  
 128 the representation<sup>42</sup>). In the case of Fig1.(b), it is a 2-fold axis (red ellipse at center of the  
 129 representation<sup>42</sup>). In both cases, two symmetry planes exist (as represented in the structures,  
 130 fig.1). Accordingly, the square rods structure has 4mm symmetry while the right-triangle  
 131 rods structure has mm2 symmetry. These symmetries are dependent on the piezoelectric

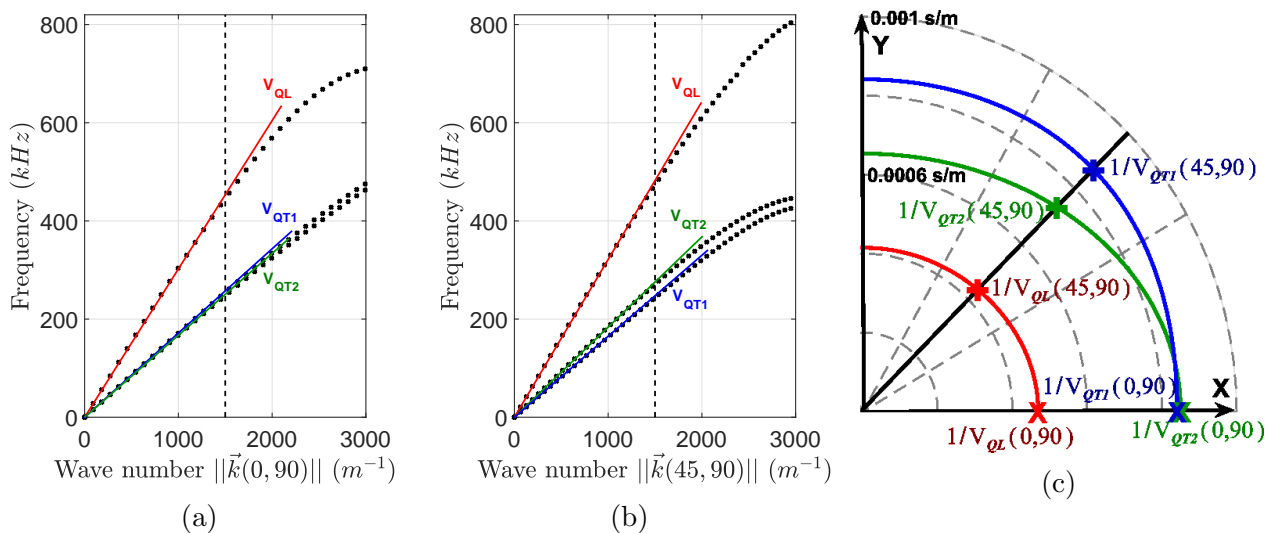


FIG. 2. Dispersion curves in the mm2-structure for 2 different wave vectors (a)  $\vec{k}(0, 90)$ , colinear to  $\vec{k}_x$  and (b)  $\vec{k}(45, 90)$ . (c) The final slowness curves for  $\|\vec{k}\| = 50\text{m}^{-1}$ ,  $0^\circ < \varphi < 90^\circ$  and  $\theta = 90^\circ$ .  $V_{QL}$ ,  $V_{QT1}$  and  $V_{QT2}$  are group velocities for, respectively, quasi-longitudinal, first quasi-transversal and second quasi-transversal modes. Calculation is performed with PZT-4<sup>43</sup> and Epoxy resin<sup>44</sup> for a 1mm-side RVE and a piezoelectric volume fraction  $v_f = 50\%$ .

132 material used for rods (here, the standard 6mm-symmetry ceramic). Parallelepipedic RVEs  
 133 of each structure are represented in Fig1 for both cases as blue dotted lines. These RVEs  
 134 possess the same symmetry as that defined previously for the two structures. To respect the  
 135 orthotropic axis of 13PC, for the mm2 structure, local basis (OXYZ) is rotated through  $45^\circ$   
 136 from the local axis of the 4mm structure. Moreover, the unit propagation vector  $\vec{n}$  is defined  
 137 by the angles  $\theta$  and  $\varphi$  in the local basis (fig.1.(c)) and  $n_1$  (resp.  $n_2, n_3$ ) is the projection of  
 138  $\vec{n}$  on  $X$ -axis (resp.  $Y$ -axis,  $Z$ -axis):

$$n_1 = \sin\theta\cos\varphi, n_2 = \sin\theta\sin\varphi, n_3 = \cos\theta. \quad (2)$$

139 For the FEM calculations, ATILA software was used<sup>46</sup>. The whole problem domains  
140 are divided into elements connected by nodes, where constitutive equations are locally ap-  
141 proximated. 1mm-side RVE is chosen. In fact, this is a typical size in  $XY$ -plane for 13PC  
142 in medical application. The reader is reminded that there is no variation of phases in the  
143  $z$ -direction, so the size has no effect on the final results. Isoparametric elements are used  
144 with quadratic interpolation along the element's sides. Hexahedrons are used with 20 nodes  
145 (8 for the corners and 12 for the middle of the edge) for the 4mm-structure. Similarly,  
146 prisms are used with 15 nodes (6 for the corners and 9 for the middle of the edge) for the  
147 mm2-structure. Furthermore, the finite element formulation used in ATILA relying upon  
148 quadratic interpolation functions, the classical  $\lambda/4$  criterion must be verified in the whole  
149 mesh to ensure the validity of the finite element result. The  $\lambda/4$  states that the largest  
150 length of each element in a given mesh has to be smaller than a quarter of the wavelength  
151 in the material for the working frequency. For structures studied in this paper, the mesh  
152 has been chosen in order to respect this criterion. Moreover, the study of periodic 13PC  
153 structure is greatly simplified by the Bloch-Floquet theorem because only one RVE needs  
154 to be meshed<sup>36</sup>.

## 155 *2. From dispersion curves to slowness curves*

156 To establish slowness curves for our two studied structures, properties of PZT-4<sup>43</sup> and  
157 Epoxy resin<sup>44</sup> in table II were chosen for the two 13PC phases. Dispersion curves were  
158 initially calculated for a 1mm-side RVE with a piezoelectric volume fraction of 50% and only  
159 the 3 lowest modes in frequency to be in accordance with the long wavelength approximation.

160 Dispersion curves were calculated for one specific direction of a wave vector in the first  
 161 Brillouin zone using modal analysis. Wave vector  $\vec{k}$  is defined by  $\vec{k}(\varphi, \theta) = k_x \cdot \vec{n}_1 + k_y \cdot \vec{n}_2 +$   
 162  $k_z \cdot \vec{n}_3$ , where:

163 -  $\varphi \in [-180^\circ, 180^\circ]$ ,

164 -  $\theta \in [0^\circ, 180^\circ]$  and if  $\theta = 90^\circ$ ,  $\vec{k} \in (XY)$ -plane,

165 In fig.2, an example of how the slowness curves are determined is put forward for two specific  
 166 propagation directions in the  $XY$ -plane ( $\vec{k}(0, 90)$  and  $\vec{k}(45, 90)$ ) and for the mm2-structure  
 167 with a step of  $91\text{m}^{-1}$  for  $\|\vec{k}\|$ . Specifically, it is shown in fig.2(a) and fig.2(b), the quasi-  
 168 longitudinal (QL), first quasi-transverse (QT1) and second quasi-transverse (QT2) modes,  
 169 where QT1 (resp. QT2) mode has an out-plane (resp. in-plane) transverse polarization in the  
 170 studied plane (here, the  $XY$ -plane). A linear behavior exists at low frequency for the three  
 171 modes where the phase velocity is equal to the group velocity ( $V_{QL}, V_{QT1}, V_{QT2}$ ). Calculating  
 172 dispersion curves for the whole characteristic volumetric region due to mm2 symmetries  
 173 ( $0^\circ < \varphi < 90^\circ$  and  $0^\circ < \theta < 90^\circ$ ), the limit of this linear region is approximatively  $\|\vec{k}\| \simeq$   
 174  $1500\text{m}^{-1}$ . This limit is indicated in fig.2(a) and (b) with the vertical dotted line. To stay  
 175 within this volumetric linear region,  $\|\vec{k}\|$  was fixed to  $50\text{m}^{-1}$  for the rest of the study. In  
 176 fig.2(c), final slowness curves (inverse of velocities) are displayed for one quarter of the  
 177  $XY$ -plane ( $0^\circ < \varphi < 90^\circ$  and  $\theta = 90^\circ$ ). The six velocities calculated from fig.2(a) and (b)  
 178 are added to slowness curves (crossed points). For FEM calculation, all the slowness points  
 179 were calculated in this way with a step of  $1^\circ$  for  $\varphi$  and  $\theta$ .

180 **B. Homogeneous structure**

181 From the numerical slowness curves in the heterogeneous material, analytical slowness  
 182 curves in a homogeneous material had to be established for a further comparison between  
 183 the two media. A general case is described for the mm2 structure in the following subsection.  
 184 As in section II A, the medium was considered to be infinite and comprised of piezoelectric  
 185 material.

186 **1. Wave equation in piezoelectric materials**

187 Starting from the expression of the mechanical strain  $T_{ij}$  (eq.1) and removing the elec-  
 188 trical potential dependency, the wave equation in a piezoelectric infinite medium can be  
 189 written<sup>42,47</sup>:

$$\rho \frac{\partial^2 u_l}{\partial t^2} = c_{ijkl}^E \frac{e_{kij} e_{jkl}}{\epsilon_{jk}^S} \frac{\partial^2 u_l}{\partial n_j \partial n_k} \quad (3)$$

190 where  $u_i$  is the component of the mechanical displacement vector  $\vec{u}$  on the axis  $n_i$  and the  
 191 time  $t$ .  $\rho$  is the density of the medium of propagation. In the assumption of a plane wave  
 192 propagation problem in an infinite medium in the  $n_j$  direction and for the eq.(3), a solution  
 193 can be written as:

$$u_i = u_i^0 e^{j\omega(t - \frac{n_j x_j}{V})} = u_i^0 F(t - \frac{n_j x_j}{V}) \quad (4)$$

194 where  $u_i^0$  is the wave polarization and  $V$  the phase velocity. When this solution is included  
 195 in eq.3, the wave equation extended to piezoelectric medium becomes:

$$\rho V^2 u_i^0 = (\Gamma_{il} + \frac{\gamma_i \gamma_l}{\epsilon}) u_l^0 \quad (5)$$

196 where  $\Gamma_{il} = c_{ijkl}^E n_j n_k$ ,  $\gamma_i = e_{kij} n_j n_k$  and  $\epsilon = \epsilon_{jk}^S n_j n_k$ . The  $(\Gamma_{il} + \frac{\gamma_i \gamma_l}{\epsilon})$  term is called the  
 197 piezoelectric Christoffel tensor and written as:

$$\bar{\Gamma}_{il} = \begin{bmatrix} \bar{\Gamma}_{11} & \bar{\Gamma}_{12} & \bar{\Gamma}_{13} \\ \bar{\Gamma}_{12} & \bar{\Gamma}_{22} & \bar{\Gamma}_{23} \\ \bar{\Gamma}_{13} & \bar{\Gamma}_{12} & \bar{\Gamma}_{33} \end{bmatrix} \quad (6)$$

198 Eq.5 is an eigenvalues equation where the wave polarization  $u_l^0$  is the eigenvector of  $\bar{\Gamma}_{il}$  with  
 199 its eigenvalue  $\lambda = \rho V^2$ . As  $\bar{\Gamma}_{il}$  is symmetrical, eigenvalues are real and to provide real  
 200 velocities, eigenvalues must also be positive. Eigenvectors are orthogonal because of the  
 201 symmetry of  $\bar{\Gamma}_{il}$ . Therefore, solving eq.5 is equivalent to finding the roots of equation:

$$|\bar{\Gamma}_{il} - \rho V^2 \delta_{il}| = 0 \quad (7)$$

202 where  $\delta_{il}$  is the Kronecker symbol. Eq.7 has three solutions for a given propagation direction  
 203  $\vec{n}$  that are velocities from the 3 known plane waves QL, QT1 and QT2 (i.e., section II A 2).

## 204 **2. mm2-structure (right-triangular rods 13PC)**

205 As mentionned earlier, the most general case is developed in this section. A mm2  
 206 piezoelectric material is characterized by 17 independent parameters: 9 elastic coefficients  
 207  $(c_{11}^E, c_{12}^E, c_{13}^E, c_{22}^E, c_{23}^E, c_{33}^E, c_{44}^E, c_{55}^E, c_{66}^E)$ , 5 piezoelectric coefficients  $(e_{15}, e_{24}, e_{31}, e_{32}, e_{33})$  and 3  
 208 dielectric parameters  $(\epsilon_{11}^S, \epsilon_{22}^S, \epsilon_{33}^S)$ . In comparison, a 4mm-structure is described by 5 elastic,  
 209 3 piezoelectric and 3 dielectric independent parameters. For both cases, all components of  
 210 the piezoelectric Christoffel tensors are analytically determined (Appendix A).

211 From these expressions, velocities  $V_{QL}$ ,  $V_{QT1}$  and  $V_{QT2}$  can be determined using eq.7 for any

212 direction. Depending on the symmetry class, calculations for all directions is not always  
 213 necessary and can be restricted. For a mm2-structure, three planes of propagation are suf-  
 214 ficient:  $XY$ -plane,  $XZ$ -plane and  $YZ$ -plane. Solutions for the  $XY$ -plane are described in  
 215 detail here and the two other planes in Appendix B.

216 In the  $XY$ -plane, the components of the projection vector  $\vec{n}$  are given by:

$$n_1 = \cos\varphi, n_2 = \sin\varphi, n_3 = 0. \quad (8)$$

217 A direct consequence of this is the zero value for the  $\bar{\Gamma}_{13}$  and  $\bar{\Gamma}_{23}$  terms in the Christoffel  
 218 tensor and a simplification of the expression for  $\bar{\Gamma}_{11}$ ,  $\bar{\Gamma}_{12} = \bar{\Gamma}_{21}$ ,  $\bar{\Gamma}_{22}$  and  $\bar{\Gamma}_{33}$  components.  
 219 Consequently, eq.7 is reduced to:

$$(\bar{\Gamma}_{33} - \lambda) \left[ (\bar{\Gamma}_{11} - \lambda) (\bar{\Gamma}_{22} - \lambda) - \bar{\Gamma}_{12}^2 \right] = 0 \quad (9)$$

220 where  $\lambda = \rho V_i^2$  are eigenvalues. The three solutions of eq.9 are:

$$\begin{cases} \lambda = \bar{\Gamma}_{33} \\ \lambda_{\pm} = \frac{1}{2} \left[ \bar{\Gamma}_{11} + \bar{\Gamma}_{22} \pm \sqrt{(\bar{\Gamma}_{11} + \bar{\Gamma}_{22})^2 - 4(\bar{\Gamma}_{11}\bar{\Gamma}_{22} - \bar{\Gamma}_{12}^2)} \right] \end{cases} \quad (10)$$

221 To assign the solutions to the correct polarizations (i.e., QL, QT1 or QT2 mode), eigenvectors  
 222 are determined. As an example, one can describe the expression of the simplest solution  
 223 for the  $XY$ -plane is detailed as:  $\lambda = \bar{\Gamma}_{33}$ . Substituting  $\bar{\Gamma}_{33}$  by its definition, the complete  
 224 expression of the corresponding velocity becomes:

$$V_{QT2}^2 = \frac{1}{\rho} \left[ c_{55}^E \cos^2\varphi + c_{44}^E \sin^2\varphi + \frac{(e_{15} \cos^2\varphi + e_{24} \sin^2\varphi)^2}{\epsilon_{11}^S \cos^2\varphi + \epsilon_{22}^S \sin^2\varphi} \right] \quad (11)$$

225 Doing the same for  $V_{QT1}$  and  $V_{QL}$  (with the two other eigenvalue expressions), the slowness  
 226 curves can be analytically calculated for a homogeneous piezoelectric material in the 3 planes  
 227 of interest for a mm2 symmetry case.



### 228 III. HOMOGENEOUS EQUIVALENT STRUCTURE

229 The symmetry class of the equivalent homogeneous structure must be the same as the ini-  
230 tial heterogeneous structure (here 13PC) and this condition must be taken into account when  
231 defining all the components of the  $\bar{c}^E$ ,  $\bar{e}$  and  $\bar{\epsilon}^S$  tensors. Overlined variables are components  
232 of the homogeneous equivalent structure. In general, if the symmetry class is unknown, the  
233 most general triclinic class is chosen by default. In the present case, a mm2-symmetry class  
234 was retained because right-triangular rods are PZT4 with 6mm-symmetry class. The ob-  
235 jective was to deduce all the effective components of the elastic, piezoelectric and dielectric  
236 tensors with a comparison of the slowness curves obtained by the two approaches (hetero-  
237 geneous and homogeneous materials materials) described earlier. This determination of all  
238 the parameters is performed in two steps. The first step involves the direct determination  
239 of several elastic parameters. A fitting process of slowness curves involving calculation by  
240 FEM is described, in a second step (section II A). The two step are detailed below. The  
242 homogenization process relies on numerical slowness curves calculated by FEM. The case of  
243 the mm2-structure (fig.1(b)) with a volume fraction ( $v_f$ ) of 50% is presented and numerical  
244 slowness curves are presented on fig.3.

#### 245 A. Step 1: analytical determination of elastic constants.

246 For specific directions in any plane ( $0^\circ$ ,  $45^\circ$ ,  $90^\circ$ ), the analytical expressions of velocities  
247 (section II B) are simplified to enable the determination of some elastic constants. For  
248 instance, in the  $XY$ -plane where general equations ( $\varphi$ -dependence) are given by the system

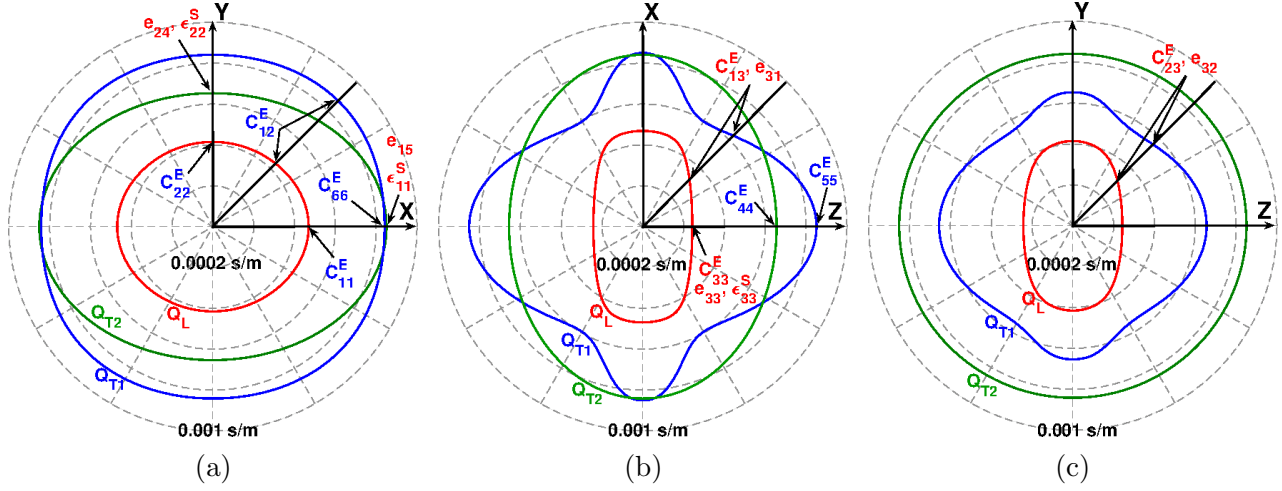


FIG. 3. Numerical slowness curves for three orthogonal planes from the same mm2-structure. Calculation is performed with PZT-4<sup>46</sup> and Epoxy resin<sup>44</sup> for a 1mm-side RVE and a piezoelectric volume fraction  $v_f = 50\%$ .

249 (10), and when  $\varphi = 0^\circ$  and  $\theta = 90^\circ$ , velocities are expressed by:

$$\begin{cases} V_{QT2}^2(0, 90) = \frac{1}{\rho} \left[ \bar{c}_{55}^E + \frac{\bar{e}_{15}^2}{\bar{e}_{11}^S} \right] \\ V_{QT1}^2(0, 90) = \frac{\bar{c}_{66}^E}{\rho} \\ V_{QL}^2(0, 90) = \frac{\bar{c}_{11}^E}{\rho} \end{cases} \quad (12)$$

250 From this set of equations the numerical values from dispersion curves (fig.3(a)) at  $\varphi = 0^\circ$   
 251 and  $\theta = 90^\circ$ ,  $\bar{c}_{11}^E$  and  $\bar{c}_{66}^E$  are easily determined. Similarly,  $\bar{c}_{55}^E$  can be resolved in the case  
 252 of a purely elastic medium ( $\bar{e}_{15} = 0$ ) but by taking into account the piezoelectricity, three  
 253 unknowns:  $\bar{c}_{55}^E$ ,  $\bar{e}_{15}$  and  $\bar{e}_{11}^S$  are added. In a similar way, some elastic constants can be  
 254 determined for other directions:  $\bar{c}_{22}^E$  in the direction  $\vec{n}(90, 90)$  on the  $1/V_{QL}$  curve and  $\bar{c}_{12}^E$   
 255 in the direction  $\vec{n}(45, 90)$  on the  $1/V_{QL}$  and  $1/V_{QT2}$  curves. In general, all elastic constants  
 256 that can be determined are added to fig.3 in blue color. Other constants that cannot

257 be analytically and independently determined like  $\bar{\epsilon}_{15}$  and  $\bar{\epsilon}_{11}^S$ , are shown in red. Finally,  
 258  $\bar{c}_{55}^E$  is no longer an unknown value because it can be determined in the  $\vec{n}(0,0)$  direction  
 259 ( $XZ$ -plane) on  $1/V_{QT2}$  curve. The same analysis is performed on the  $XZ$ - and  $YZ$ -planes  
 260 (fig.3). Several effective tensor components appear in different directions but in order not  
 261 to overload fig.3, these are displayed only once. For example, it can be observed that  $\bar{c}_{55}^E$   
 262 appears both in the expressions of  $V_{QT2}(0,90)$  (system 12) and  $V_{QT2}(0,0)$  (fig.3(b)). All the  
 263 six parameters that can be determined analytically are summarized in table I. The same  
 264 table is applicable for the 4mm-structure, except that the (90,90)-direction and the QT1  
 265 mode from the (90,90)-direction are not necessary, for this symmetry structure.

266 Finally, for the mm2-symmetry, with three orthogonal planes and six different directions,  
 267 a system of nine independent equations is achieved with 11 unknowns. Here, the full deter-  
 268 mination of tensor components is not analytically possible. Consequently, the second step  
 269 is a numerical determination performed by a fitting process.

## 270 **B. Step 2: fitting process.**

271 For a full determination of effective tensors, eleven constants have to be fitted:  $\bar{c}_{13}^E$ ,  $\bar{c}_{23}^E$ ,  $\bar{c}_{33}^E$ ,  
 272 all the five constants of  $\bar{\epsilon}$  tensor and the three constants of  $\bar{\epsilon}^S$  tensor. The fitting process by  
 273 the objective function (OF) that is minimized and the settings for the optimization algorithm  
 274 (OA) are described below. Both slowness and velocity are used interchangeably throughout  
 275 the text because once one is determined, the other one is simultaneously determined too.

TABLE I. Analytical expressions for particular directions used for determining six elastic constants in mm2-structure.

	$(\varphi, \theta)$	Mode	$\rho V_{QL,QT1,QT2} =$
XY-plane	(0,90)	$Q_L$	$\bar{c}_{11}^E$
		$Q_{T1}$	$\bar{c}_{66}^E$
	(90,90)	$Q_L$	$\bar{c}_{22}^E$
	(45,90)	$Q_L, Q_{T1}$	$\frac{A+B}{4} \pm \frac{[(A+B)^2 - AB + (\bar{c}_{12}^E + \bar{c}_{66}^E)^2]^{\frac{1}{2}}}{4}$ with $A = (\bar{c}_{11}^E + \bar{c}_{66}^E)$ , $B = (\bar{c}_{22}^E + \bar{c}_{66}^E)$
XZ-	(0,0)	$Q_{T1}$	$\bar{c}_{55}^E$
		$Q_{T2}$	$\bar{c}_{44}^E$

276 **1. Objective function**

277 The aim of this process is to fit the analytical velocities from a homogeneous medium  
 278 onto numerical velocities considered as the reference from heterogeneous medium. Therefore,  
 279 one needs to minimize the difference between the numerical velocities  $v_{ij_{\text{FEM}}}$  and analytical  
 280 velocities  $v_{ij_{\text{Chris}}}$  for all propagation directions of the three planes of interest for the mm2-  
 281 symmetry. Specifically,  $v_{ij_{\text{FEM}}}$  are gleaned from section II A 2 while  $v_{ij_{\text{Chris}}}$  are calculated for  
 282 each iteration from equations established in section II B 2 with the new set of parameters  
 283 to be fitted (unknown components of effective tensors). For each new set, a score  $S_a$  is

284 calculated by the OF using the least squares method:

$$S_a = \sum_{i=1}^M \left( \sum_{j=1}^N \frac{(v_{ij\text{FEM}} - v_{ij\text{Chris}})^2}{N \langle v_{ij\text{FEM}}^2 \rangle} \right) \quad (13)$$

285 where  $M$  is the number of slowness curves selected for the fitting process ( $M = 5$  for the  
 286 mm2-structure and  $M = 3$  for the 4mm-structure) and  $N$  is the number of propagation di-  
 287 rections used (with a default of  $N = 360$ ). Finally,  $\langle \rangle$  is the mean symbol. The five specific  
 288 curves (fig.4) were specifically chosen because the remaining unknowns that must be deter-  
 289 mined are involved in their analytical expressions (see red constants on fig3). 4mm-structure  
 290 requires fewer slowness curves to be fitted because there are fewer effective independent com-  
 291 ponents, in a similar way to the simplification of table I for this case, as explained earlier.

292

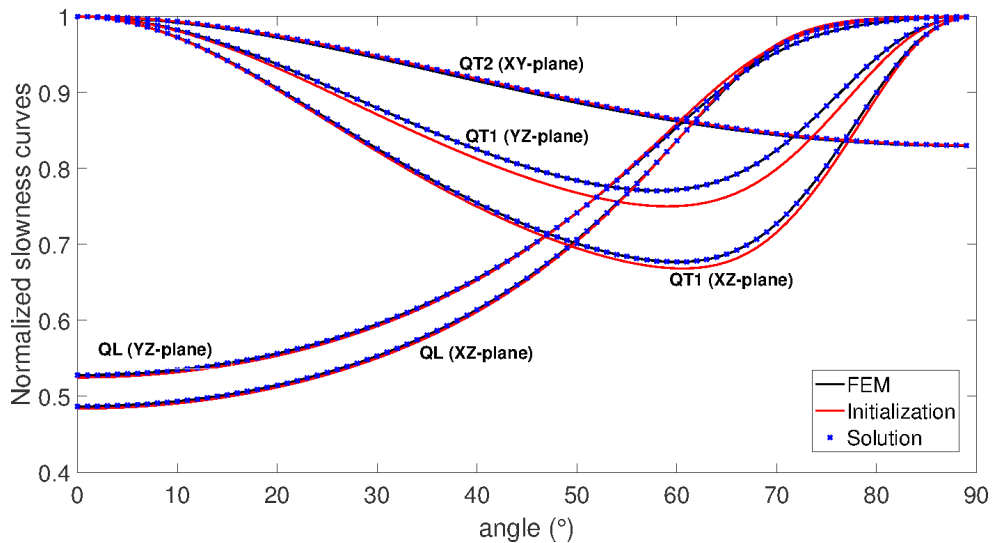


FIG. 4. Selected slowness curves ( $M=5$ ) for the fitting process displayed on one quarter of the plane ( $\varphi, \theta \in [0^\circ 90^\circ]$ ).

293

294

295 **2. Optimization algorithm**

296 The OA selects a new set of parameters based on all previous scores returned by OF for  
 297 the different sets, previously selected. The time needed to reach the best optimization score  
 298 is called rate of convergence. In order to achieve a fast convergence rate, an OA based on a  
 299 canonical search is preferred. Here the Nelder-Mead algorithm<sup>48</sup>, also known as the simplex  
 300 method was used.

301 In the case of a mm2-structure, the set of effective parameters to be determined is de-  
 302 scribed by the vector  $x = \{\bar{c}_{13}^E, \bar{c}_{23}^E, \bar{c}_{33}^E, \bar{e}_{31}, \bar{e}_{32}, \bar{e}_{33}, \bar{e}_{24}, \bar{e}_{15}, \bar{\epsilon}_{11}^S, \bar{\epsilon}_{22}^S, \bar{\epsilon}_{33}^S\}$ . One of the drawbacks  
 303 of using this kind of OA is the requirement of an initial vector ( $x_{\text{init}}$ ) to start the process.  
 304 Values of  $x_{\text{init}}$  are set with the matrix method<sup>11</sup> that provides a good approximation for  
 305 longitudinal tensor (subscripts 33) but a weak approximation of the transverse tensors pa-  
 306 rameters. It is worth mentioning that these values are calculated as a function of the 13PC  
 307 volume fraction of piezoelectric phase.

308 The second setting for the algorithm is the definition of the search-space limits. These  
 309 are contained in the boundary vectors  $x_{\text{UB}}$  for the upper boundaries and  $x_{\text{LB}}$  for the lower  
 310 boundaries. Here, the choice of a large search-space is preferred and boundary vectors are  
 311 defined by  $x_{\text{UB}} = 5x_{\text{init}}$  and  $x_{\text{LB}} = 0.01x_{\text{init}}$ .

312 In fig.4, the five selected slowness curves for the fitting process are represented only on  
 313 one quarter of their planes for the case  $v_f = 50\%$ . The curves are normalized to their own  
 314 maximum to highlight the differences. The black curves that almost coincide with the dotted

315 blue lines are the FEM calculations. The red curves are the initial slowness curves of the  
 316 OA and were calculated using  $x_{\text{init}}$  in table II.

TABLE II. Case  $v_f = 50\%$ . Elastic ( $c^E$  in GPa), piezoelectric ( $e$  in C.m<sup>-2</sup>), dielectric ( $\epsilon^S$  in  $/\epsilon_0$ ) constants and density ( $\rho$  in kg/m<sup>3</sup>) for PZT4<sup>43</sup> ceramic, Epoxy<sup>44</sup> resin, mm2- and 4mm- structures calculated by the present method and by the FFT method. Initial vector  $x_{\text{init}}$  for the OA and relative differences between FFT and present methods are also given. Star (resp. cross and dash) indicates constants analytically determined on first step (resp. non-value parameter and known parameters from others values).

Constants		$c_{11}^E$	$c_{12}^E$	$c_{13}^E$	$c_{22}^E$	$c_{23}^E$	$c_{33}^E$	$c_{44}^E$	$c_{55}^E$	$c_{66}^E$	$e_{15}$	$e_{24}$	$e_{31}$	$e_{32}$	$e_{33}$	$\epsilon_{11}^S$	$\epsilon_{22}^S$	$\epsilon_{33}^S$	$\rho$
PZT-4		139	77.8	74.3	-	-	115.4	25.6	-	30.6	12.7	-	-5.2	-	15.1	730	-	635	7500
Epoxy resin		7.84	3.9	-	-	-	-	-	-	-	-	-	-	-	-	3	-	-	1100
Constants		$\bar{c}_{11}^E*$	$\bar{c}_{12}^E*$	$\bar{c}_{13}^E$	$\bar{c}_{22}^E*$	$\bar{c}_{23}^E$	$\bar{c}_{33}^E$	$\bar{c}_{44}^E*$	$\bar{c}_{55}^E*$	$\bar{c}_{66}^E*$	$\bar{e}_{15}$	$\bar{e}_{24}$	$\bar{e}_{31}$	$\bar{e}_{32}$	$\bar{e}_{33}$	$\bar{\epsilon}_{11}^S$	$\bar{\epsilon}_{22}^S$	$\bar{\epsilon}_{33}^S$	$\bar{\rho}$
$x_{\text{init}}$		×	×	7.56	×	7.56	40	×	×	×	0.0039	0.0039	-0.27	-0.27	9.15	6	6	333	×
mm2	this work	16.04	8.43	8.28	18.85	9.16	41.50	6.90	4.76	4.98	0.0136	0.0195	-0.33	-0.36	8.69	8	12	332	4300
	FFT	16.28	8.58	8.40	19.12	9.37	40.88	7.00	4.85	5.07	0.0112	0.037	-0.33	-0.40	9.07	10	10	326	-
	rel. dif.(%)	1.54	1.81	1.62	1.41	2.35	1.50	1.47	1.85	1.79	19.3	61.9	0.51	11.6	4.25	18.5	12.2	1.71	-
4mm	this work	19.37	6.37	8.64	-	-	40	5.57	-	3.92	0.0075	-	-0.273	-	9.14	5	-	332	4300
	FFT	19.25	6.39	8.66	-	-	40.73	5.53	-	3.9	0.0167	-	-0.353	-	9.08	9	-	332	-
	rel. dif.(%)	0.62	0.31	0.23	-	-	1.81	0.72	-	0.51	76	-	25.6	-	0.66	57	-	0	-

318 **IV. RESULTS AND DISCUSSION**

319 Homogenization results are presented for two different cases: (1) results for a specific  
 320 volume fraction ( $v_f$ ) of 50% for 4mm and mm2 13PC are presented in the first section, (2)  
 321 parameter variation as a function of  $v_f$  are shown in second section. In both sections, all  
 322 results are compared with the FFT method for validation. The principle of this numerical  
 323 scheme is briefly recalled in Appendix C.

324 **A. Specific case of  $v_f = 50\%$**

325 The volume fraction of  $v_f = 50\%$  was chosen because it is a typical 13PC value employed  
 326 for medical imaging applications. This value allows for the optimization of the thickness  
 327 coupling coefficient ( $k_t$ ) which is an essential parameter for transducer design<sup>3</sup>. Variations  
 328 of  $v_f$  are possible (typically between 30% and 90%) depending on the desired optimized  
 329 properties. Fig.4 shows the solution found by the fitting process (blue dotted lines). The  
 330 maximum difference between the initialization and the FEM is located on the QL wave  
 331 in the  $XZ$ -plane at  $62^\circ$  and its value is 2.98%. After the fitting process, the solution  
 332 presents a maximum difference on the QT2 wave in the  $XY$ -plane, equal to 0.3% (equating  
 333 to 10 fold reduction when compared to  $x_{\text{init}}$ ). It is also noticeable that the curves from  
 334 the QT2 wave in the  $XY$ -plane was unchanged between  $x_{\text{init}}$  and the solution. In fact,  
 335 this curve is governed by Eq.11. OA can only modify variables  $\bar{e}_{24}$ ,  $\bar{e}_{15}$   $\bar{\epsilon}_{11}^S$  and  $\bar{\epsilon}_{22}^S$  in this  
 336 equation as  $\bar{c}_{44}^E$  and  $\bar{c}_{55}^E$  are already determined and considered fixed values. Essentially, the  
 337 problem is that, in Eq.11, the term  $\frac{(e_{15}\cos^2\varphi + e_{24}\sin^2\varphi)^2}{\epsilon_{11}^S\cos^2\varphi + \epsilon_{22}^S\sin^2\varphi}$  is approximately 500 times smaller



338 than  $c_{55}^E \cos^2 \varphi + c_{44}^E \sin^2 \varphi$ . This means that at least for this case, the variables  $\bar{e}_{24}$ ,  $\bar{e}_{15}$ ,  $\bar{e}_{11}^S$   
 339 and  $\bar{e}_{22}^S$  are not highly sensitive. As a result, OA had no influence on them.

340 In table II, all effective tensor components from the solution are given in the case of  
 341 the 4mm-structure (fig.1(a)) and the mm2-structure (fig.1(b)). For comparative purposes,  
 342 the same components obtained by the FFT method are also presented. As expected from  
 343 the previous paragraph, large relative differences appear for  $\bar{e}_{24}$ ,  $\bar{e}_{15}$ ,  $\bar{e}_{11}^S$  and  $\bar{e}_{22}^S$  until 62%.  
 344 However, these differences are not of critical concern because, in practice, these parameters  
 345 do not affect the expected behavior of 13PC functions either in thickness or flexural modes.  
 346 To reduce these differences, additional work needs to be performed during OF selection, by  
 347 for example, adding another slowness curve for the fit or giving extra-weight for this QT2  
 348 slowness curve.

## 349 B. Results for $v_f$ variations

350 In this section, the homogenization method is performed on different volume fractions  
 351 (10%, 30%, 50% and 70%) and compared with the FFT method. In fig.5, the elastic con-  
 352 stants calculated from the present study (black crosses) are well evaluated for the most  
 353 effective constants ( $< 2\%$ ). In fact, the largest relative difference with the FFT method (red  
 354 circles) appears to be 6% for  $\bar{c}_{44}^E$  at  $v_f = 70\%$ . This difference is not significant when com-  
 355 pared with the  $\bar{c}_{44}^E$  value of 24% for 4mm-structure (blue crosses). However, these variations  
 356 of elastic constants show that the shapes have a stronger effect on the constant characteristics  
 357 of the  $x$ -axis ( $\bar{c}_{11}^E$ ) as compared with  $\bar{c}_{22}^E$  on the  $y$ -axis and  $\bar{c}_{33}^E$  on the  $z$ -axis.

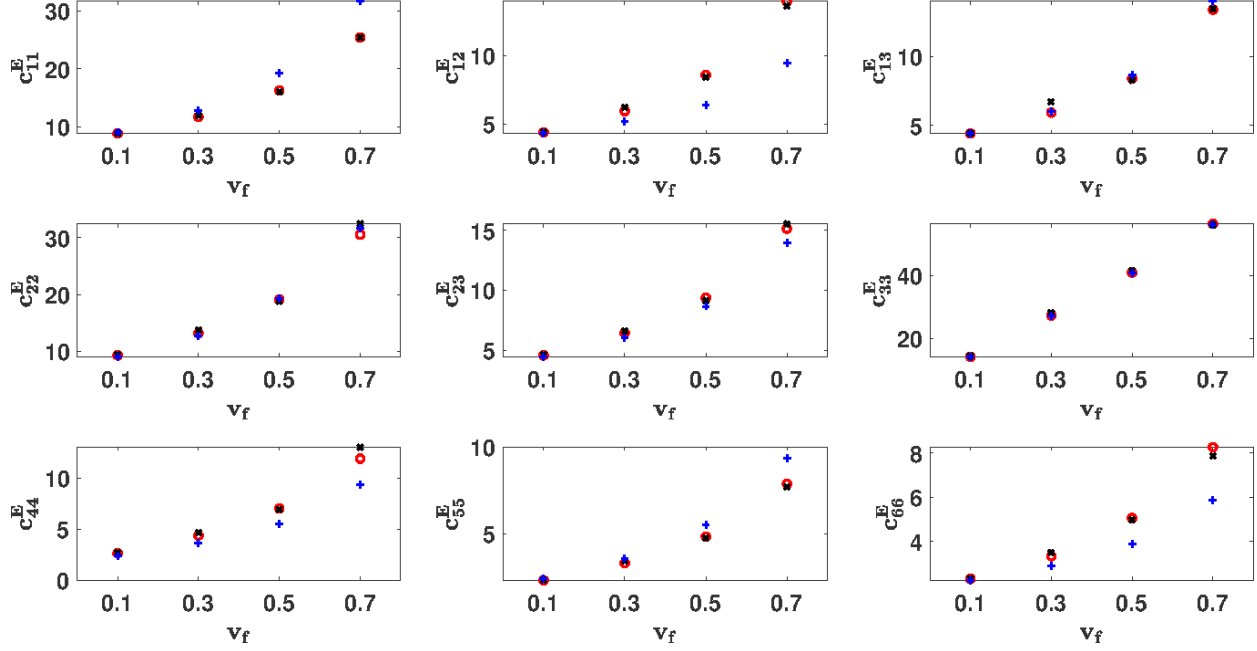


FIG. 5. Effective elastic constants (in GPa) as a function of piezoelectric volume fraction ( $v_f$ ) from the present study represented with the black cross for mm2-structure and blue plus-sign for 4mm-structure. Results from FFT numerical scheme (red circles) are also added for the mm2-structure.

358 Fig.6 shows homogenized piezoelectric and dielectric effective parameters. The gap be-  
 359 tween the FFT and the present method on  $\bar{e}_{24}$  and  $\bar{e}_{15}$  was unexpectedly negligible for the  
 360 reasons already explained in paragraph IV A. However, this difference was pronounced for  
 361 the higher volume fractions. Details on the constants' sensitivity are extensively covered by  
 362 Balé<sup>47</sup>.

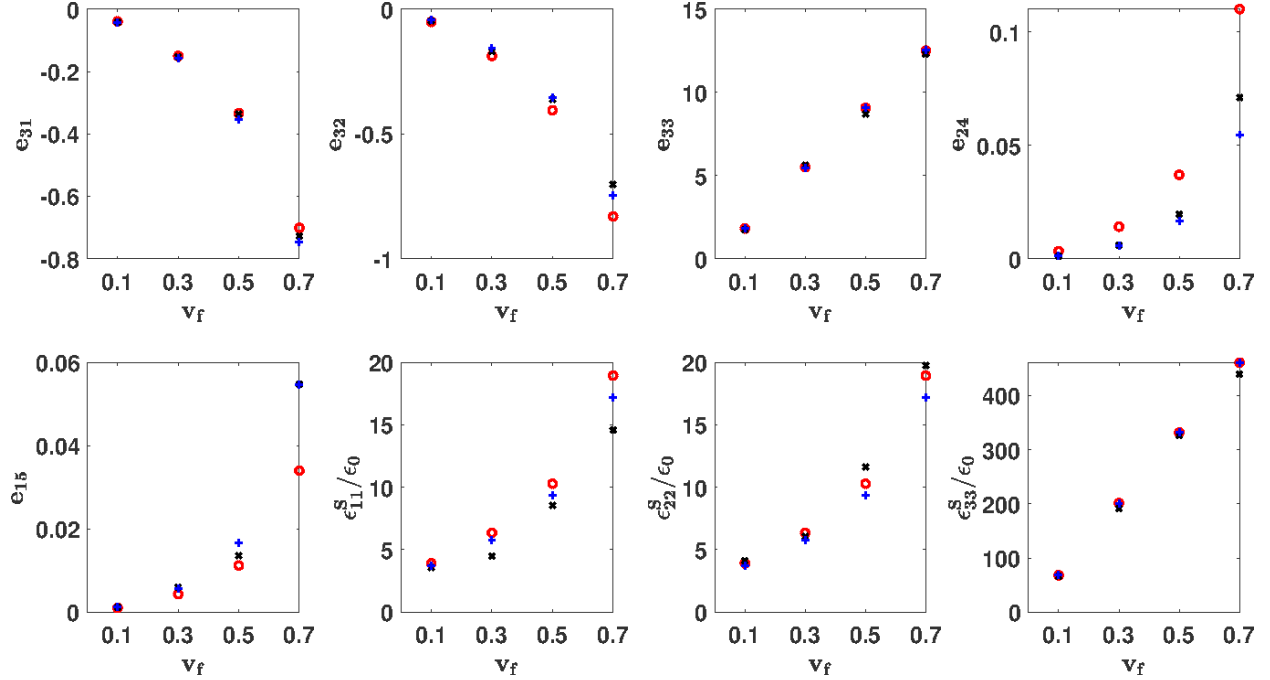


FIG. 6. Homogenized piezoelectric (in  $C.m^{-2}$ ) and dielectric coefficients (in  $/\epsilon_0$ ) from the present study represented with the black cross for mm2-structure and blue plus sign for 4mm-structure. Results from FFT method is also added with red circle for mm2-structure. Variations are according to volume fraction  $v_f$ .

365 **C. Simplification for an experimental homogenization: example of the 4mm-**  
 366 **structure**

367 In order to apply the present method to an experimental setup, particular effort has to  
 368 be expended on the acquisition of 13PC slowness curves for the 3 planes of interest. In  
 369 fact, in the theoretical methodology (general case), 13PC slowness curves were calculated  
 370 using FEM in all directions at incremental steps of  $1^\circ$ . Unfortunately, measurements made  
 371 this way, are extremely laborious but also unnecessary. Rather the objective is to find a  
 372 trade-off between the number of measurements and the accuracy of the deduced effective

373 tensors. The example of a 4mm-structure was chosen here because it is the most frequently  
 374 used in practice.

375 As shown in section III A, specific directions are necessary to determine several constants  
 376 analytically: for the 4mm-structure in the  $XY$ -plane,  $x$ -direction and  $(45, 90)$ -direction pro-  
 377 vide the constants  $\bar{c}_{11}^E$ ,  $\bar{c}_{12}^E$ ,  $\bar{c}_{66}^E$  and the  $z$ -direction in the  $XZ$ -plane (or  $YZ$ -plane) brings the  
 378  $\bar{c}_{44}^E$  value. Hence, these three directions are retained. Moreover, the fitting process (section  
 379 III B) for the 4mm-structure has to determine the constants  $\bar{c}_{13}^E$ ,  $\bar{c}_{33}^E$ ,  $\bar{e}_{15}$ ,  $\bar{e}_{31}$ ,  $\bar{e}_{33}$ ,  $\bar{\epsilon}_{11}$  and  
 380  $\bar{\epsilon}_{33}$ . These constants appear in two specific directions of the  $XZ$ -plane (or  $YZ$ -plane):

- 381 •  $z$ -direction (already retained at step 1) for  $\bar{c}_{33}^E$ ,  $\bar{e}_{33}$  and  $\bar{\epsilon}_{33}$  on the QL mode,
- 382 • and  $(0, 45)$ - or  $(90, 45)$ -direction for the rest on the QL and QT1 modes.

383 To ensure the validity of the effective parameters obtained using a reduced number of di-  
 384 rections (reduced case), the relative difference between these values and the general case  
 385 must not exceed 5%. This limit was arbitrarily chosen. Using only the  $(0, 45)$ -direction in  
 386 addition to the three  $((0, 90), (45, 90)$  and  $(0, 0))$  for the analytical determination, results  
 387 were compared with the general case (45 directions in 2 planes = 90 directions) and, were  
 388 generally correct for all volume fractions (10%, 30%, 50% and 70%) with relative differences  
 389 lower than 10% except for  $e_{15}$  due to difficulties explained in section IV A. In table III, the  
 390 30% volume fraction case is presented because it is the case which exhibits the highest rel-  
 391 ative differences. Only the fitted parameters are presented because parameter determined  
 392 by analytical method is, by definition, always equal. It is noticeable that the final results  
 393 deteriorate with relative differences of 93% for the  $e_{31}$  value and 72% for  $e_{15}$ . This also

394 confirms that substantial experimental information is lost, with a reduction in angles. The  
 395 objective then is to add a few more experimental data to see whether the accuracy of the  
 396 final results can be improved.

TABLE III. Effective elastic  $\bar{c}^E$  (GPa), piezoelectric  $\bar{e}$  (C.m<sup>-2</sup>) and dielectric  $\bar{\epsilon}^S$  ( $/\epsilon_0$ ) constant of 4mm-structure ( $v_f = 30\%$ ).

Properties	general case	reduced cases	
	90 directions	4 directions (rel. diff. %)	6 directions (rel. diff. %)
$c_{13}^E$	6,01	6,71 (12)	6,00 (0.1)
$c_{33}^E$	28,08	26,68 (4)	27,87 (1)
$e_{15}$	3,54e-4	0.0001 (72)	1,78e-4 (30)
$e_{31}$	-0.14	-0,27 (93)	-0,14 (0)
$e_{33}$	5,35	5,52 (3)	5,25 (2)
$\epsilon_{11}^S/\epsilon_0$	5,81	6,08 (5)	5,56 (4)
$\epsilon_{33}^S/\epsilon_0$	202	194 (4)	200 (1)

397  
 398

399 For the algorithm, there is a lack of accuracy evaluated on constants calculated from the  
 400 QL and QT1 modes in (0, 45)-direction. Consequently, two additional directions: (0, 30)-  
 401 and (0, 60)-directions are considered. In this way, the algorithm is better able to reveal the  
 402 velocity variations in this plane. These results are also shown in table III (6 directions).

403 As expected, relative differences declined with a maximum of 4% (except for the  $e_{15}$  value).  
 404 With these three cases, the logical trend of increasing accuracy, coupled with the increase  
 405 in measured directions, are highlighted. Finally, when angle reductions are applied to the  
 406 experimental setup, the user is obliged to consider choosing a trade-off between the number  
 407 of measured directions and accuracy of the effective constants.

## 408 V. CONCLUSION

409 A method based on wave propagation was successfully implemented to determine the  
 410 effective electroelastic moduli of 1-3 piezocomposites. Slowness curves in several planes  
 411 were used to identify all the parameters, whose, Christoffel tensors were analytically ex-  
 412 pressed. This procedure was performed in two main steps. First, several elastic constants  
 413 (listed in table II with stars) in particular directions were directly determined using the  
 414 quasi-longitudinal and two quasi-transversal modes. Second, to complete generation of the  
 415 effective data (constants without star in table II) a fitting process using the Nelder-Mead  
 416 algorithm was performed. In this study, two piezoelectric rod shapes (square and right-  
 417 triangle) that can be designed by the well-known “Dice and Fill” method were selected.  
 418 These two configurations belong to 4mm and mm2 symmetry class, respectively. For the  
 419 second and most general case, requiring the determination of 17 constants, 10 ( $\bar{c}_{11}^E$ ,  $\bar{c}_{12}^E$ ,  $\bar{c}_{13}^E$ ,  
 420  $\bar{c}_{22}^E$ ,  $\bar{c}_{33}^E$ ,  $\bar{c}_{44}^E$ ,  $\bar{c}_{55}^E$ ,  $\bar{c}_{66}^E$ ,  $\bar{e}_{31}$  and  $\bar{e}_{33}^S$ ) were obtained with an accuracy of less than 2%. Larger  
 421 differences were obtained for the two dielectric and two piezoelectric constants ( $\bar{e}_{24}$ ,  $\bar{e}_{15}$ ,  $\bar{e}_{11}^S$   
 422 and  $\bar{e}_{22}^S$ ) however, these values have limited influence for most applications using thickness  
 423 or flexural modes. To validate our approach, the results were compared with a Fourier

424 transform-based numerical homogenization scheme for quasi-static conditions. The idea be-  
 425 hind this development was to use this method in *operating conditions* for 1-3 piezocomposite  
 426 while also taking into account variations in properties, as compared to the original materials  
 427 database of each phase, appearing in the fabrication process. From a practical point of view,  
 428 we showed that with only 7 carefully chosen directions of propagation, the entire database  
 429 of 1-3 piezocomposite with 4mm symmetry can be determined. Future applications can be  
 430 guided by adaptation of this method to 1-3 piezocomposite for a given thickness and lat-  
 431 eral dimensions. Here, direct measurements of propagative Lamb waves are more suitable.  
 432 Just as the method described for volume waves, dispersion curves corresponding to the first  
 433 three symmetric and antisymmetric theoretical Lamb modes will be exploited. Specific elec-  
 434 trode designs on 1-3 piezocomposite will be used to generate modes in a particular direction  
 435 and scanning laser vibrometer can be used to measure normal displacements at the surface  
 436 specimen to deduce experimental disperse curve<sup>49</sup>. This new objective is now underway.

#### 437 **ACKNOWLEDGMENTS**

438 This work was supported by the French Research Agency (ANR HEcATE 14-CE07-0028).

#### 439 **APPENDIX A:**

440 For a piezoelectric material with mm2-symmetry, piezoelectric Christoffel tensor's com-  
 441 ponents are:

$$\bar{\Gamma}_{11} = c_{11}^E n_1^2 + c_{66}^E n_2^2 + c_{55}^E n_3^2 + \frac{(e_{15} + e_{31})^2 n_1^2 n_3^2}{\epsilon_{11}^S n_1^2 + \epsilon_{22}^S n_2^2 + \epsilon_{33}^S n_3^2}, \quad (\text{A1})$$

$$\bar{\Gamma}_{12} = (c_{12}^E + c_{66}^E)n_1n_2 + \frac{(e_{15} + e_{31})n_1n_3(e_{24} + e_{32})n_2n_3}{\epsilon_{11}^S n_1^2 + \epsilon_{22}^S n_2^2 + \epsilon_{33}^S n_3^2}, \quad (\text{A2})$$

$$\bar{\Gamma}_{13} = (c_{13}^E + c_{55}^E)n_1n_3 + \frac{(e_{15} + e_{31})n_1n_3(e_{15}n_1^2 + e_{24}n_2^2 + e_{33}n_3^2)}{\epsilon_{11}^S n_1^2 + \epsilon_{22}^S n_2^2 + \epsilon_{33}^S n_3^2}, \quad (\text{A3})$$

$$\bar{\Gamma}_{22} = c_{66}^E n_1^2 + c_{22}^E n_2^2 + c_{44}^E n_3^2 + \frac{(e_{24} + e_{32})^2 n_2^2 n_3^2}{\epsilon_{11}^S n_1^2 + \epsilon_{22}^S n_2^2 + \epsilon_{33}^S n_3^2}, \quad (\text{A4})$$

$$\bar{\Gamma}_{23} = (c_{23}^E + c_{44}^E)n_2n_3 + \frac{(e_{24} + e_{32})n_2n_3(e_{15}n_1^2 + e_{24}n_2^2 + e_{33}n_3^2)}{\epsilon_{11}^S n_1^2 + \epsilon_{22}^S n_2^2 + \epsilon_{33}^S n_3^2}, \quad (\text{A5})$$

$$\bar{\Gamma}_{33} = c_{55}^E n_1^2 + c_{44}^E n_2^2 + c_{33}^E n_3^2 + \frac{(e_{15}n_1^2 + e_{24}n_2^2 + e_{33}n_3^2)^2}{\epsilon_{11}^S n_1^2 + \epsilon_{22}^S n_2^2 + \epsilon_{33}^S n_3^2}. \quad (\text{A6})$$

442 **APPENDIX B:**

443 Expression of the six velocities for  $XZ$ -plane and  $YZ$ -plane according to the solutions of  
444 equation 7:

-  $XZ$ -plane:

$$n_1 = \sin\theta, n_2 = 0, n_3 = \cos\theta$$

445 Solutions are:

$$\begin{cases} V_{QT2}^2 = \frac{\bar{\Gamma}_{22}}{\rho} \\ V_{QL,QT1}^2 \pm = \frac{\bar{\Gamma}_{11} + \bar{\Gamma}_{33} \pm \sqrt{(\bar{\Gamma}_{11} + \bar{\Gamma}_{33})^2 - 4(\bar{\Gamma}_{11}\bar{\Gamma}_{33} - \bar{\Gamma}_{13}^2)}}{2\rho} \end{cases} \quad (\text{B1})$$

-  $YZ$ -plane:

$$n_1 = 0, n_2 = \sin\theta, n_3 = \cos\theta$$



$$\begin{cases} V_{QT2}^2 = \frac{\bar{\Gamma}_{11}}{\rho} \\ V_{QL,QT1}^2 \pm = \frac{\bar{\Gamma}_{22} + \bar{\Gamma}_{33} \pm \sqrt{(\bar{\Gamma}_{22} + \bar{\Gamma}_{33})^2 - 4(\bar{\Gamma}_{22}\bar{\Gamma}_{33} - \bar{\Gamma}_{23}^2)}}{2\rho} \end{cases} \quad (\text{B2})$$

447 **APPENDIX C:**

448 Considering the unit-cell  $\Omega$  of a periodic piezoelectric media, the quasi-static heteroge-  
449 neous local problem reads,  $\forall \mathbf{x} \in \Omega$ ,

$$\begin{cases} \text{curl}(\text{curl}^T \mathbf{S}(\mathbf{x})) = \mathbf{0}, & \text{div } \mathbf{T}(\mathbf{x}) = \mathbf{0}, \\ \text{curl } \mathbf{E}(\mathbf{x}) = \mathbf{0}, & \text{div } \mathbf{D}(\mathbf{x}) = \mathbf{0}, \end{cases} \quad (\text{C1})$$

450 with coupled constitutive equations (1)

$$\mathbf{T} = \mathbf{c}^E : \mathbf{S} - \mathbf{e}^T \cdot \mathbf{E}, \quad \mathbf{D} = \boldsymbol{\epsilon}^S \cdot \mathbf{E} + \mathbf{e} : \mathbf{S} \quad (\text{C2})$$

451 and imposed periodicity conditions on the local fields on the boundary of the unit-cell  $\Omega$ .

452 Making use of the Green functions method, the solution fields are expressible as coupled

453 Lippmann-Schwinger equations<sup>39</sup>

$$\begin{cases} \mathbf{S}(\mathbf{x}) = \langle \mathbf{S} \rangle_{\Omega} - \boldsymbol{\Gamma}^0 * \boldsymbol{\tau}(\mathbf{x}) \\ \mathbf{E}(\mathbf{x}) = \langle \mathbf{E} \rangle_{\Omega} - \boldsymbol{\Delta}^0 * \mathbf{P}(\mathbf{x}) \end{cases} \quad (\text{C3})$$

454 with  $\boldsymbol{\Gamma}^0$  and  $\boldsymbol{\Delta}^0$  the Green operators corresponding to a uniform reference material with

455 elastic tensor  $\mathbf{c}^0$  and dielectric tensor  $\boldsymbol{\epsilon}^0$ .  $\langle \cdot \rangle_{\Omega}$  indicate the volume average over the unit-cell.

456 The fields  $\boldsymbol{\tau}$  and  $\mathbf{P}$  are given by

$$\begin{cases} \boldsymbol{\tau}(\mathbf{x}) = (\mathbf{c}^E(\mathbf{x}) - \mathbf{c}^0) : \mathbf{S}(\mathbf{x}) - \mathbf{e}^T(\mathbf{x}) \cdot \mathbf{E}(\mathbf{x}) \\ \mathbf{P}(\mathbf{x}) = \mathbf{e}(\mathbf{x}) : \mathbf{S}(\mathbf{x}) + (\boldsymbol{\epsilon}^S(\mathbf{x}) - \boldsymbol{\epsilon}^0) \cdot \mathbf{E}(\mathbf{x}). \end{cases} \quad (\text{C4})$$

457 The solution fields (C3) can be expressed in Fourier space and the problem is solved using  
458 an adequate iterative procedure<sup>38,39</sup>. The effective electroelastic coefficients tensors  $\tilde{\mathbf{c}}^E$ ,  $\tilde{\mathbf{e}}$   
459 and  $\tilde{\boldsymbol{\epsilon}}^S$  are defined by

$$\langle \mathbf{T} \rangle_{\Omega} = \tilde{\mathbf{c}}^E : \langle \mathbf{S} \rangle_{\Omega} - \tilde{\mathbf{e}}^T \cdot \langle \mathbf{E} \rangle_{\Omega}, \quad \langle \mathbf{D} \rangle_{\Omega} = \tilde{\boldsymbol{\epsilon}}^S \cdot \langle \mathbf{E} \rangle_{\Omega} + \tilde{\mathbf{e}} : \langle \mathbf{S} \rangle_{\Omega} \quad (\text{C5})$$

## 460 References

- 461 <sup>1</sup>R. Newnham, D. Skinner, and L. Cross, “Connectivity and piezoelectric-  
462 pyroelectric composites,” *Materials Research Bulletin* **13**(5), 525–536 (1978)  
463 <https://linkinghub.elsevier.com/retrieve/pii/0025540878901617> doi:  
464 [10.1016/0025-5408\(78\)90161-7](https://doi.org/10.1016/0025-5408(78)90161-7).
- 465 <sup>2</sup>W. A. Smith and B. A. Auld, “Modeling 1-3 composite piezoelectrics: thickness-mode  
466 oscillations.,” *IEEE transactions on ultrasonics, ferroelectrics, and frequency control* **38**(1),  
467 40–7 (1991) <http://www.ncbi.nlm.nih.gov/pubmed/18267555> doi: [10.1109/58.67833](https://doi.org/10.1109/58.67833).
- 468 <sup>3</sup>M. Lethiecq, F. Levassort, D. Certon, and L. P. Tran-Huu-Hue, “Piezoelec-  
469 tric Transducer Design for Medical Diagnosis and NDE,” in *Piezoelectric and*  
470 *Acoustic Materials for Transducer Applications* (Springer US, Boston, MA, 2008),  
471 pp. 191–215, [http://link.springer.com/10.1007/978-0-387-76540-2\\_{\\_}10](http://link.springer.com/10.1007/978-0-387-76540-2_{_}10), doi:  
472 [10.1007/978-0-387-76540-2\\_10](https://doi.org/10.1007/978-0-387-76540-2_10).

- 473 <sup>4</sup>W. Voigt, “Ueber die Beziehung zwischen den beiden Elasticitätsconstanten  
474 isotroper Körper,” *Annalen der Physik* **274**(12), 573–587 (1889)  
475 <http://doi.wiley.com/10.1002/andp.18892741206> doi: 10.1002/andp.18892741206.
- 476 <sup>5</sup>A. Reuss, “Berechnung der Fließgrenze von Mischkristallen auf Grund der Plas-  
477 tizitätsbedingung für Einkristalle .,” *ZAMM - Zeitschrift für Angewandte Mathematik*  
478 und *Mechanik* **9**(1), 49–58 (1929) <http://doi.wiley.com/10.1002/zamm.19290090104>  
479 doi: 10.1002/zamm.19290090104.
- 480 <sup>6</sup>P. Bisegna and R. Luciano, “Variational bounds for the overall properties of piezoelectric  
481 composites,” *J. Mech. Phys. Solids* **44**, 583–602 (1996).
- 482 <sup>7</sup>H. Banno, “Theoretical Equations for Dielectric and Piezoelectric Properties of Fer-  
483 roelectric Composites Based on Modified Cubes Model,” *Japanese Journal of Ap-*  
484 *plied Physics* **24**(S2), 445 (1985) <http://stacks.iop.org/1347-4065/24/445> doi:  
485 10.7567/JJAPS.24S2.445.
- 486 <sup>8</sup>K. Hashimoto and M. Yarnaguchi, “Elastic, Piezoelectric and Dielectric Prop-  
487 erties of Composite Materials,” in *IEEE 1986 Ultrasonics Symposium*, IEEE  
488 (1986), pp. 697–702, <http://ieeexplore.ieee.org/document/1535764/>, doi:  
489 10.1109/ULTSYM.1986.198824.
- 490 <sup>9</sup>H. Chan and J. Unsworth, “Simple model for piezoelectric ceramic/polymer  
491 1-3 composites used in ultrasonic transducer applications,” *IEEE Transactions*  
492 *on Ultrasonics, Ferroelectrics and Frequency Control* **36**(4), 434–441 (1989)  
493 <http://ieeexplore.ieee.org/document/31780/> doi: 10.1109/58.31780.

494 <sup>10</sup>H. Banno, “Theoretical Equations for Dielectric, Piezoelectric and Elastic Properties of a  
495 0–3 Composite Based on Modified Cubes Model–A General Solution–,” Japanese Journal  
496 of Applied Physics **28**(S2), 190 (1989) <http://stacks.iop.org/1347-4065/28/190> doi:  
497 [10.7567/JJAPS.28S2.190](https://doi.org/10.7567/JJAPS.28S2.190).

498 <sup>11</sup>F. Levassort, M. Lethiecq, D. Certon, and F. Patat, “A matrix method  
499 for modeling electroelastic moduli of 0-3 piezo-composites,” IEEE Transactions  
500 on Ultrasonics, Ferroelectrics and Frequency Control **44**(2), 445–452 (1997)  
501 <http://ieeexplore.ieee.org/document/585129/> doi: [10.1109/58.585129](https://doi.org/10.1109/58.585129).

502 <sup>12</sup>J. Eshelby, “The determination of the elastic field of an ellipsoidal inclu-  
503 sion, and related problems,” Proceedings of the Royal Society of London.  
504 Series A. Mathematical and Physical Sciences **241**(1226), 376–396 (1957)  
505 <https://royalsocietypublishing.org/doi/10.1098/rspa.1957.0133> doi:  
506 [10.1098/rspa.1957.0133](https://doi.org/10.1098/rspa.1957.0133).

507 <sup>13</sup>W. Deeg, “The analysis of dislocation, crack, and inclusion problems in piezoelectric solids,”  
508 Ph.D. thesis, Stanford University, 1980.

509 <sup>14</sup>M. Dunn and M. Taya, “An analysis of piezoelectric composite materials con-  
510 taining ellipsoidal inhomogeneities,” Proceedings of the Royal Society of Lon-  
511 don. Series A: Mathematical and Physical Sciences **443**(1918), 265–287 (1993)  
512 <https://royalsocietypublishing.org/doi/10.1098/rspa.1993.0145> doi:  
513 [10.1098/rspa.1993.0145](https://doi.org/10.1098/rspa.1993.0145).

- 514 <sup>15</sup>T. Mori and K. Tanaka, “Average stress in matrix and average elastic en-  
515 ergy of materials with misfitting inclusions,” *Acta Metallurgica* **21**(5), 571–  
516 574 (1973) <https://linkinghub.elsevier.com/retrieve/pii/0001616073900643> doi:  
517 [10.1016/0001-6160\(73\)90064-3](https://doi.org/10.1016/0001-6160(73)90064-3).
- 518 <sup>16</sup>Y. Benveniste, “The determination of the elastic and electric fields in a piezo-  
519 electric inhomogeneity,” *Journal of Applied Physics* **72**(3), 1086–1095 (1992)  
520 <http://aip.scitation.org/doi/10.1063/1.351784> doi: [10.1063/1.351784](https://doi.org/10.1063/1.351784).
- 521 <sup>17</sup>W. Biao, “Three-dimensional analysis of an ellipsoidal inclusion in a piezo-  
522 electric material,” *International Journal of Solids and Structures* **29**(3), 293–  
523 308 (1992) <https://linkinghub.elsevier.com/retrieve/pii/0020768392902014> doi:  
524 [10.1016/0020-7683\(92\)90201-4](https://doi.org/10.1016/0020-7683(92)90201-4).
- 525 <sup>18</sup>H. Berger, S. Kari, U. Gabbert, R. Rodriguez-Ramos, R. Guinovart, J. A.  
526 Otero, and J. Bravo-Castillero, “An analytical and numerical approach for cal-  
527 culating effective material coefficients of piezoelectric fiber composites,” *In-*  
528 *ternational Journal of Solids and Structures* **42**(21-22), 5692–5714 (2005)  
529 <https://linkinghub.elsevier.com/retrieve/pii/S0020768305001277> doi:  
530 [10.1016/j.ijsolstr.2005.03.016](https://doi.org/10.1016/j.ijsolstr.2005.03.016).
- 531 <sup>19</sup>A. A. Bent and N. W. Hagood, “Piezoelectric Fiber Composites with Interdig-  
532 itated Electrodes,” *Journal of Intelligent Material Systems and Structures* **8**(11),  
533 903–919 (1997) <http://journals.sagepub.com/doi/10.1177/1045389X9700801101> doi:  
534 [10.1177/1045389X9700801101](https://doi.org/10.1177/1045389X9700801101).

535 <sup>20</sup>C. Poizat and M. Sester, “Effective properties of composites with embedded  
536 piezoelectric fibres,” *Computational Materials Science* **16**(1-4), 89–97 (1999)  
537 <https://linkinghub.elsevier.com/retrieve/pii/S0927025699000506> doi:  
538 [10.1016/S0927-0256\(99\)00050-6](https://doi.org/10.1016/S0927-0256(99)00050-6).

539 <sup>21</sup>H. E. Pettermann and S. Suresh, “A comprehensive unit cell model:  
540 a study of coupled effects in piezoelectric 1–3 composites,” *Inter-  
541 national Journal of Solids and Structures* **37**(39), 5447–5464 (2000)  
542 <https://linkinghub.elsevier.com/retrieve/pii/S0020768399002243> doi:  
543 [10.1016/S0020-7683\(99\)00224-3](https://doi.org/10.1016/S0020-7683(99)00224-3).

544 <sup>22</sup>E. Lenglet, A.-C. Hladky-Hennion, and J.-C. Debus, “Numerical homogenization tech-  
545 niques applied to piezoelectric composites,” *The Journal of the Acoustical Society of  
546 America* **113**(2), 826–833 (2003) <http://asa.scitation.org/doi/10.1121/1.1537710>  
547 doi: [10.1121/1.1537710](https://doi.org/10.1121/1.1537710).

548 <sup>23</sup>H. Berger, S. Kari, U. Gabbert, R. Rodriguez-Ramos, J. Bravo-Castillero,  
549 R. Guinovart-Diaz, F. J. Sabina, and G. A. Maugin, “Unit cell models of  
550 piezoelectric fiber composites for numerical and analytical calculation of ef-  
551 fective properties,” *Smart Materials and Structures* **15**(2), 451–458 (2006)  
552 <http://stacks.iop.org/0964-1726/15/i=2/a=026?key=crossref.9f57e8e0ef4a86f7fcf2693e6043>  
553 doi: [10.1088/0964-1726/15/2/026](https://doi.org/10.1088/0964-1726/15/2/026).

554 <sup>24</sup>T. Enab, “Evaluation of the Effective Electromechanical Properties of Unidirectional  
555 Piezocomposites Using Different Representative Volume Elements,” *International Jour-  
556 nal of Mechanical and Mechatronics Engineering* **15**(2), 21–29 (2015).

- 557 <sup>25</sup>S. Kari, H. Berger, R. Rodriguez-Ramos, and U. Gabbert, “Numerical Evaluation of Effective Material Properties of Transversely Randomly Distributed Unidirectional Piezoelectric Fiber Composites,” *Journal of Intelligent Material Systems and Structures* **18**(4), 559 361–372 (2007) <http://journals.sagepub.com/doi/10.1177/1045389X06066293> doi: 560 [10.1177/1045389X06066293](http://dx.doi.org/10.1177/1045389X06066293). 561
- 562 <sup>26</sup>R. Kar-Gupta and T. A. Venkatesh, “Electromechanical response of 1-3 piezoelectric composites: Effect of poling characteristics,” *Journal of Applied Physics* **98**(5), 054102 (2005) 563 <http://aip.scitation.org/doi/10.1063/1.2014933> doi: [10.1063/1.2014933](http://dx.doi.org/10.1063/1.2014933). 564
- 565 <sup>27</sup>S. Aimmanee, and H. Asanuma, “Micromechanics-based predictions of effective 566 properties of a 1-3 piezocomposite reinforced with hollow piezoelectric fibers,” *Mechanics of Advanced Materials and Structures* **27**(22), 1873–1887 (2020) 567 <https://www.tandfonline.com/doi/full/10.1080/15376494.2018.1529842> doi: 568 [10.1080/15376494.2018.1529842](http://dx.doi.org/10.1080/15376494.2018.1529842). 569
- 570 <sup>28</sup>Y. Zhang, L. Wang and L. Qin, “Equivalent parameter model of 1-3 piezo- 571 composite with a sandwich polymer,” *Results in Physics* **9**, 1256–1261 (2018) 572 <https://linkinghub.elsevier.com/retrieve/pii/S2211379717317515> doi: 573 [10.1016/j.rinp.2018.04.046](http://dx.doi.org/10.1016/j.rinp.2018.04.046).
- 574 <sup>29</sup>H. Savakus, K. Klicker, and R. Newnham, “PZT-epoxy piezoelectric transduc- 575 ers: A simplified fabrication procedure,” *Materials Research Bulletin* **16**(6), 677– 576 680 (1981) <http://linkinghub.elsevier.com/retrieve/pii/0025540881902671> doi: 577 [10.1016/0025-5408\(81\)90267-1](http://dx.doi.org/10.1016/0025-5408(81)90267-1).

578 <sup>30</sup>R. Rouffaud, A.-C. Hladky-Hennion, and F. Levassort, “A combined genetic algorithm  
579 and finite element method for the determination of a practical elasto-electric set for 1-3  
580 piezocomposite phases,” *Ultrasonics* **77** (2017) doi: [10.1016/j.ultras.2017.02.015](https://doi.org/10.1016/j.ultras.2017.02.015).

581 <sup>31</sup>Y. C. Chu and S. I. Rokhlin, “Stability of determination of composite mod-  
582 uli from velocity data in planes of symmetry for weak and strong anisotropies,”  
583 *The Journal of the Acoustical Society of America* **95**(1), 213–225 (1994)  
584 <http://asa.scitation.org/doi/10.1121/1.408378> doi: [10.1121/1.408378](https://doi.org/10.1121/1.408378).

585 <sup>32</sup>C. Potel, J. de Belleval, and Y. Gargouri, “Floquet waves and classical plane waves in  
586 an anisotropic periodically multilayered medium: Application to the validity domain of  
587 homogenization,” *The Journal of the Acoustical Society of America* **97**(5), 2815–2825  
588 (1995) <http://asa.scitation.org/doi/10.1121/1.411849> doi: [10.1121/1.411849](https://doi.org/10.1121/1.411849).

589 <sup>33</sup>L. Wang and S. I. Rokhlin, “Floquet wave homogenization of periodic anisotropic  
590 media,” *The Journal of the Acoustical Society of America* **112**(1), 38–45 (2002)  
591 <http://asa.scitation.org/doi/10.1121/1.1488942> doi: [10.1121/1.1488942](https://doi.org/10.1121/1.1488942).

592 <sup>34</sup>M. Wilm, S. Ballandras, V. Laude, and T. Pastureauud, “A full 3D plane-wave-expansion  
593 model for 1-3 piezoelectric composite structures,” *The Journal of the Acoustical Society of*  
594 *America* **112**(3), 943–952 (2002) <http://asa.scitation.org/doi/10.1121/1.1496081>  
595 doi: [10.1121/1.1496081](https://doi.org/10.1121/1.1496081).

596 <sup>35</sup>G. Ferin, D. Certon, N. Felix, and F. Patat, “Experimental and theoretical de-  
597 termination of 1–3 piezocomposite electroacoustic tensor,” *Ultrasonics* **44**, e763–  
598 e772 (2006) <https://linkinghub.elsevier.com/retrieve/pii/S0041624X06001259>



599 doi: [10.1016/j.ultras.2006.05.090](https://doi.org/10.1016/j.ultras.2006.05.090).

600 <sup>36</sup>P. Langlet, A. Hladky-Hennion, and J. Decarpigny, “Analysis of the propaga-  
601 tion of plane acoustic waves in passive periodic materials using the finite element  
602 method,” *The Journal of the Acoustical Society of America* **98**(5), 2792–2800 (1995)  
603 <http://asa.scitation.org/doi/10.1121/1.413244> doi: [10.1121/1.413244](https://doi.org/10.1121/1.413244).

604 <sup>37</sup>H. Moulinec and P. Suquet, “A numerical method for computing the over-  
605 all response of nonlinear composites with complex microstructure,” *Com-  
606 puter Methods in Applied Mechanics and Engineering* **157**(1-2), 69–94 (1998)  
607 <https://linkinghub.elsevier.com/retrieve/pii/S0045782597002181> doi:  
608 [10.1016/S0045-7825\(97\)00218-1](https://doi.org/10.1016/S0045-7825(97)00218-1).

609 <sup>38</sup>R. Brenner, “Numerical computation of the response of piezoelectric  
610 composites using fourier transform,” *Physical Review B* **79**(18), 184106  
611 (2009) <https://link.aps.org/doi/10.1103/PhysRevB.79.184106> doi:  
612 [10.1103/PhysRevB.79.184106](https://doi.org/10.1103/PhysRevB.79.184106).

613 <sup>39</sup>R. Brenner, “Computational approach for composite materials with coupled constitutive  
614 laws,” *Zeitschrift für angewandte Mathematik und Physik* **61**, 919–927,1420–9039 (2010).

615 <sup>40</sup>R. Brenner, J. Bravo-Castillero, and D. M. Léon, “Investigation of the effective response  
616 of 2-1-2 piezoelectric composites,” *Procedia IUTAM* **3**, 292–300 (2012).

617 <sup>41</sup>T. Ikeda, *Fundamentals of Piezoelectricity* (Oxford University Press, New York, 1996).

618 <sup>42</sup>D. Royer and E. Dieulesaint, *Elastic Waves in Solids I: Free and Guided Propagation*  
619 (Springer-Verlag Berlin, 1999).

- 620 <sup>43</sup>McGrawHill, *American Institute of Physics Handbook*, 2ème édité ed. (1963).
- 621 <sup>44</sup>M. Pham Thi, A.-C. Hladky-Hennion, H. L. Khanh, L.-P. Tran-Huu-Hue, M. Lethiecq,  
622 and F. Levassort, “Large area 0-3 and 1-3 piezoelectric composites based on sin-  
623 gle crystal PMN-PT for transducer applications,” *Physics Procedia* **3**(1), 897–  
624 904 (2010) <http://linkinghub.elsevier.com/retrieve/pii/S1875389210001161> doi:  
625 [10.1016/j.phpro.2010.01.115](https://doi.org/10.1016/j.phpro.2010.01.115).
- 626 <sup>45</sup>J. A. Brown, E. Cherin, J. H. Yin, and F. S. Foster, “Fabrication and Performance of  
627 High-Frequency Composite Transducers with Triangular-Pillar Geometry,” *Ieee Trans-*  
628 *actions on Ultrasonics Ferroelectrics and Frequency Control* **56**(4), 827–836 (2009) doi:  
629 [10.1109/tuffc.2009.1106](https://doi.org/10.1109/tuffc.2009.1106).
- 630 <sup>46</sup>ISEN, “ATILA, Finite-Element Software Package for the analysis of 2D & 3D structures  
631 based on smart materials” (2010).
- 632 <sup>47</sup>A. Balé, “Homogénéisation et caractérisation de matériaux multiphasiques piézoélectriques  
633 (composites de connectivité 1-3 et céramiques texturées) pour les transducteurs ultra-  
634 sonores sans plomb,” Ph.D. thesis, University of Tours, 2019.
- 635 <sup>48</sup>J. Nelder and R. Mead, “A simplex method for function minimization,” *Computer Journal*  
636 **7**(4), 308–313 (1965).
- 637 <sup>49</sup>J. Guyonvarch, D. Certon, L. Ratsimandresy, F. Patat, and M. Lethiecq,  
638 “Response of bare 1–3 piezocomposite array to localized electrical excitation,”  
639 *The Journal of the Acoustical Society of America* **117**(1), 200–209 (2005)  
640 <http://asa.scitation.org/doi/10.1121/1.1829259> doi: [10.1121/1.1829259](https://doi.org/10.1121/1.1829259).